Available online at www.eccomasproceedia.org
Eccomas Proceedia COMPDYN (2023) 2050-2061

ECCOMAS
Proceedia

COMPDYN 2023
9th ECCOMAS Thematic Conference on
Computational Methods in Structural Dynamics and Earthquake Engineering
M. Papadrakakis, M. Fragiadakis (eds.)
Athens, Greece, 12-14 June 2023

NONLINEAR DYNAMIC ANALYSIS OF RIGID BODIES SUPPORTED BY RATE-INDEPENDENT HYSTERETIC ELEMENTS

Nicolò Vaiana and Luciano Rosati

Department of Structures for Engineering and Architecture, University of Naples Federico II
via Claudio 21, 80125 Naples, Italy
e-mail: nicolo.vaiana@unina.it

Abstract. *We propose a mathematical model to perform nonlinear dynamic analyses of two-dimensional rigid bodies supported by rate-independent hysteretic elements and subjected to external generalized forces or support motion. In particular, the rigid body is assumed to have an arbitrary polygonal shape and its properties are computed as functions of quantities depending upon its vertices. In addition, the rate-independent hysteretic elements may exhibit an arbitrary hysteretic behavior. The latter is modeled by using an accurate and efficient uniaxial phenomenological model, recently formulated by the authors, that allows for the simulation of complex generalized force-displacement hysteresis loops. The proposed mathematical model is adopted to carry out a nonlinear time history analysis on a mechanical system composed by a rigid body mounted on four wire rope isolators and subjected to bidirectional support acceleration.*

Keywords: Vibration Isolation System, Active Isolation, Passive Isolation, Rigid Body, Vaiana-Rosati Model.

doi: 10.7712/120123.10541.21084

1 INTRODUCTION

In the field of aerospace, civil, mechanical and naval engineering, vibration isolation systems are generally employed to reduce vibrations transmitted by a mechanical system (e.g., fans, turbines, motors, propellers) to the supporting structure (*active isolation*) or to protect a mechanical system (e.g., sensitive electrical equipment, operating tables, metrology equipment) or a structure (e.g., buildings, bridges) from vibrations induced by external generalized forces and/or support motion (*passive isolation*).

In both cases, hysteretic devices, having rate-dependent and/or rate-independent hysteretic behavior [1–6], are typically employed. The former (latter) exhibit a generalized force that does (not) depend on the device generalized velocity.

During the design process of a vibration isolation system, the results provided by nonlinear time history analyses allow one to verify and optimize the key design parameters by taking into account the real complex nonlinear behavior exhibited by the adopted hysteretic devices. Consequently, it is crucial to provide suitable methods and models to perform such sophisticated nonlinear dynamic analyses.

To this end, we propose a mathematical model made up of a rigid body supported by rate-independent hysteretic elements. The rigid body is described by a generic plane domain assumed to have a completely arbitrary polygonal shape. In particular, the properties of the rigid body are computed as functions of quantities depending upon its vertices.

On the other hand, the nonlinear behavior exhibited by the rate-independent hysteretic elements, assumed to be characterized by an arbitrary complex hysteresis loop shape, is simulated by adopting an accurate and computationally efficient uniaxial phenomenological model recently proposed by the authors [7, 8] and belonging to a more general class of hysteretic models [9–11].

The manuscript is organized into three parts. In the first one (Section 2), we introduce the proposed mathematical model and we derive its nonlinear equilibrium equations. Subsequently, in the second part (Section 3), we briefly summarize the proposed hysteretic model, and, in the third part (Section 4), we perform a nonlinear time history analysis of a rigid body mounted on four wire rope isolators and subjected to support motion.

2 MATHEMATICAL MODEL

This section briefly illustrates a mathematical model consisting of a rigid body, having arbitrary polygonal shape, supported by rate-independent hysteretic elements.

2.1 Rigid Body with Arbitrary Polygonal Shape

Let us consider a rigid body defined by a generic plane domain Ω that is characterized by a completely arbitrary polygonal shape. Assuming that the rigid body has a uniformly distributed mass m, its mass center coincides with its gravity center G.

After introducing a right-handed Cartesian coordinate system, having axes x_1, x_2, x_3, and origin at G, the i-th vertex defining the domain Ω may be identified by the point $P_i : (x_1^i, x_2^i)$. Accordingly, such a domain can be defined by a discrete set of N points that are numbered in consecutive order by circulating along the boundary $\partial\Omega$ in a counterclockwise sense, as illustrated in Figure 1a.

To fully describe the dynamic response of the rigid body, it is necessary to evaluate its second mass moment J_{x_3}, also called mass moment of inertia about the x_3 axis or, equivalently, polar

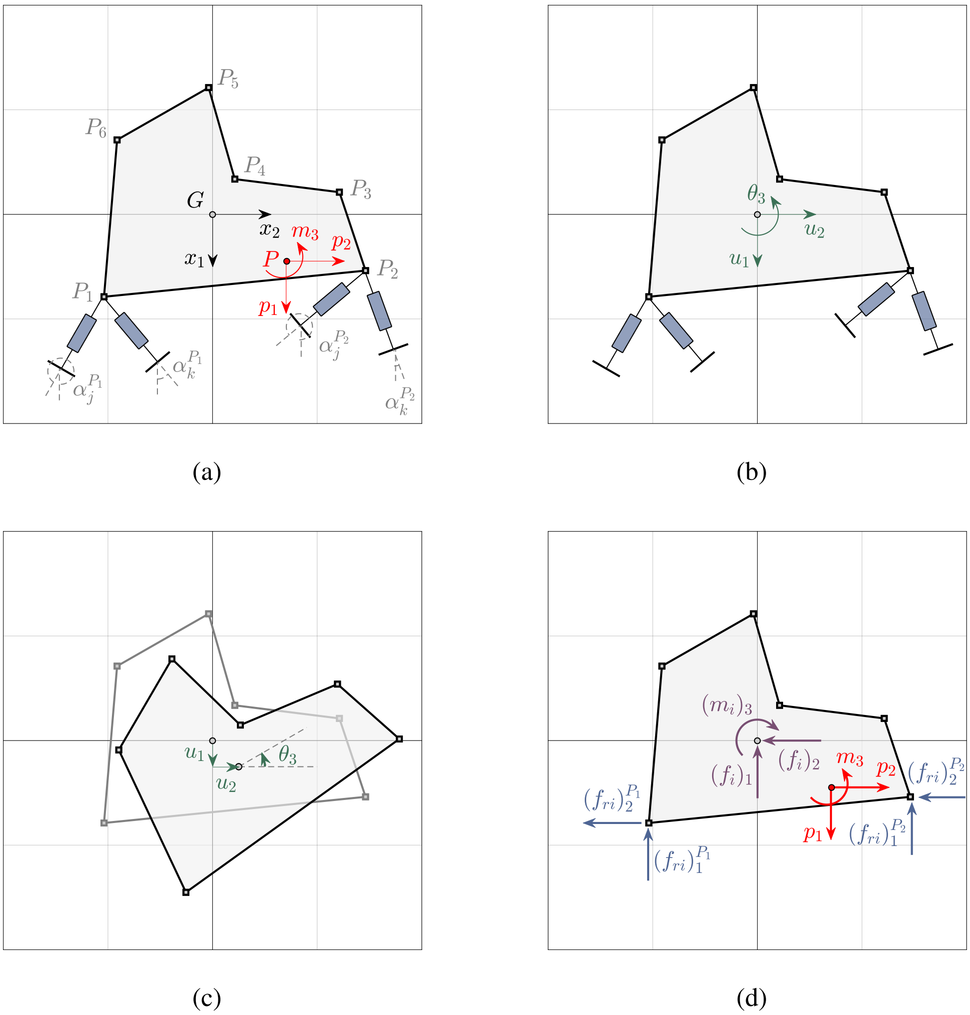

Figure 1: Mathematical model (a), generalized coordinates (b), displaced position (c), and free-body diagram (d).

moment of inertia about the origin G. In particular, J_{x_3} is defined as:

$$J_{x_3} = \frac{m}{A}\left(I_{x_1} + I_{x_2}\right), \tag{1}$$

where A is the area of the domain Ω, whereas I_{x_1} (I_{x_2}) represents the area moment of inertia about the x_1 (x_2) axis. Such terms can be expressed as finite sums of quantities depending upon the vertices of the domain Ω:

$$A = \frac{1}{2}\sum_{i=1}^{N} x_1^i x_2^{i+1} - x_2^i x_1^{i+1}, \tag{2}$$

$$I_{x_1} = \frac{1}{12}\sum_{i=1}^{N}\left(x_1^i x_2^{i+1} - x_2^i x_1^{i+1}\right)\left(x_2^i x_2^i + x_2^i x_2^{i+1} + x_2^{i+1} x_2^{i+1}\right), \tag{3}$$

$$I_{x_2} = \frac{1}{12}\sum_{i=1}^{N}\left(x_1^i x_2^{i+1} - x_2^i x_1^{i+1}\right)\left(x_1^i x_1^i + x_1^i x_1^{i+1} + x_1^{i+1} x_1^{i+1}\right), \tag{4}$$

where $x_1^{N+1} = x_1^1$ and $x_2^{N+1} = x_2^1$.

2.2 Generalized Coordinates

The generalized coordinates selected to describe the rigid body motion at the generic time t are: (i) the displacement $u_1(t)$ of the mass center along x_1 axis, (ii) the displacement $u_2(t)$ of the mass center along x_2 axis, and (iii) the rotation $\theta_3(t)$ of the rigid body about x_3 axis, as illustrated in Figures 1b and 1c. They are measured from the static equilibrium position.

2.3 Rate-Independent Hysteretic Elements

For simplicity, in the sequel, we assume to have two rate-independent hysteretic elements attached to the i-th point P_i and referred to as the j-th and k-th elements, respectively.

In particular, the j-th (k-th) element makes an angle $\alpha_j^{P_i}$ ($\alpha_k^{P_i}$) with a line that passes through P_i and is parallel to x_1 axis. In addition, it exhibits a rate-independent hysteretic force $(f_{ri})_j^{P_i}$ $\left((f_{ri})_k^{P_i}\right)$ depending on the displacement $u_j^{P_i}$ $\left(u_k^{P_i}\right)$ of point P_i along the j-th (k-th) direction.

The latter can be expressed as:

$$u_j^{P_i} = u_1^{P_i} \cos \alpha_j^{P_i} + u_2^{P_i} \sin \alpha_j^{P_i}, \tag{5}$$

$$u_k^{P_i} = u_1^{P_i} \cos \alpha_k^{P_i} + u_2^{P_i} \sin \alpha_k^{P_i}, \tag{6}$$

where the displacements $u_1^{P_i}$ and $u_2^{P_i}$ of P_i, under the hypothesis of small generalized displacements, can be written in terms of the generalized coordinates as follows:

$$u_1^{P_i} = u_1 - \theta_3 x_2^i, \tag{7}$$

$$u_2^{P_i} = u_2 + \theta_3 x_1^i. \tag{8}$$

Consequently, the components $(f_{ri})_1^{P_i}$ and $(f_{ri})_2^{P_i}$ of the resultant force acting on P_i can be calculated as:

$$(f_{ri})_1^{P_i} = (f_{ri})_j^{P_i} \cos \alpha_j^{P_i} + (f_{ri})_k^{P_i} \cos \alpha_k^{P_i}, \tag{9}$$

$$(f_{ri})_2^{P_i} = (f_{ri})_j^{P_i} \sin \alpha_j^{P_i} + (f_{ri})_k^{P_i} \sin \alpha_k^{P_i}. \tag{10}$$

Figure 1a presents an example of rigid body supported by two sets of two rate-independent hysteretic elements attached to points P_1 and P_2 respectively.

Note that the presented relations can be straightforwardly extended to the case of an arbitrary number N_{ri} of rate-independent hysteretic elements connected to the i-th point P_i.

2.4 Nonlinear Equilibrium Equations

Figure 1d shows (i) the hysteretic forces $(f_{ri})_1^{P_1}$ and $(f_{ri})_2^{P_1}$ applied at P_1, (ii) the hysteretic forces $(f_{ri})_1^{P_2}$ and $(f_{ri})_2^{P_2}$ applied at P_2, (iii) the generalized inertia forces $(f_i)_1$, $(f_i)_2$, $(m_i)_3$ applied at G, and (iv) the generalized external forces p_1, p_2, m_3 applied at point $P : (x_1^P, x_2^P)$.

By imposing the three equilibrium conditions of the rigid body at the generic time t, we get the following system of second-order nonlinear ordinary differential equations:

$$\begin{aligned}
&(f_i)_1(t) + (f_{ri})_1^{P_1}(t) + (f_{ri})_1^{P_2}(t) = p_1(t), \\
&(f_i)_2(t) + (f_{ri})_2^{P_1}(t) + (f_{ri})_2^{P_2}(t) = p_2(t), \\
&(m_i)_3(t) - (f_{ri})_1^{P_1}(t) x_2^1 - (f_{ri})_1^{P_2}(t) x_2^2 + (f_{ri})_2^{P_1}(t) x_1^1 + (f_{ri})_2^{P_2}(t) x_1^2 = p_3(t),
\end{aligned} \tag{11}$$

in which:

$$(f_i)_1(t) = m\ddot{u}_1(t), \ \ (f_i)_2(t) = m\ddot{u}_2(t), \ \ (m_i)_3(t) = J_{x_3}\ddot{\theta}_3(t), \tag{12}$$

$$p_3(t) = m_3(t) - p_1(t) x_2^P + p_2(t) x_1^P, \tag{13}$$

with J_{x_3} given by Equation (1) and $\ddot{u}_1 = d^2u_1/dt^2$, $\ddot{u}_2 = d^2u_2/dt^2$, $\ddot{\theta}_3 = d^2\theta_3/dt^2$.

3 VAIANA-ROSATI MODEL OF HYSTERESIS

In this section we briefly summarize a novel uniaxial phenomenological model, denominated Vaiana-Rosati Model (VRM) [7, 8], to compute the force $(f_{ri})_j^{P_i}$ $\left((f_{ri})_k^{P_i}\right)$ exhibited by the j-th (k-th) rate-independent hysteretic element attached to the i-th point P_i of the mathematical model illustrated in Figure 1a.

Such a hysteretic model offers a series of advantages with respect to other existing models available in the literature, such as: (i) the use of closed form expressions, or equivalent rate equations, for the evaluation of the generalized force, tangent stiffness, and work, (ii) the description of complex hysteresis loops, (iii) the independent simulation of the loading and unloading phases by means of two different sets of eight parameters, (iv) the straightforward calibration of the parameters thanks to their clear theoretical and/or experimental significance, and (v) the easy computer implementation.

In the sequel, we first describe the analytical formulation of the model and, subsequently, we illustrate its capability to reproduce four different types of complex generalized force-displacement hysteresis loops.

Please, note that the subscript j (k) and the superscript P_i, adopted to refer to the j-th (k-th) element connected to the i-th point P_i, will be omitted for simplicity.

3.1 Model Formulation

The VRM adopts the generalized displacement u (generalized force f_{ri}) as input (output) variable. In particular, at the generic time t, the generalized force f_{ri} can be computed as:

$$f_{ri}(t) = f_e(t)+k_b u(t)+s(t)f_0-[f_e(t_P) + k_b u(t_P) + s(t)f_0 - f_{ri}(t_P)]\, e^{-s(t)\alpha(u(t)-u(t_P))}, \quad (14)$$

where:

$$f_e(t) = \beta_1 e^{\beta_2 u(t)} - \beta_1 + \frac{4\gamma_1}{1+e^{-\gamma_2(u(t)-\gamma_3)}} - 2\gamma_1. \quad (15)$$

In the previous equations, s represents the sign of the generalized velocity $\dot{u}$, t_P is assumed to be, for simplicity, the time corresponding to the beginning of the generic loading or unloading phase, whereas $k_b = k_b^+(k_b^-)$, $f_0 = f_0^+(f_0^-)$, $\alpha = \alpha^+(\alpha^-)$, $\beta_1 = \beta_1^+(\beta_1^-)$, $\beta_2 = \beta_2^+(\beta_2^-)$, $\gamma_1 = \gamma_1^+(\gamma_1^-)$, $\gamma_2 = \gamma_2^+(\gamma_2^-)$, $\gamma_3 = \gamma_3^+(\gamma_3^-)$ when $s > 0$ ($s < 0$). The latter represent the eight parameters that control the generic loading (unloading) phase and need to be experimentally or numerically identified thus satisfying the following conditions: $f_0^+ > f_0^-$, $\alpha^+ > 0$ ($\alpha^- > 0$), whereas k_b^+, β_1^+, β_2^+, γ_1^+, γ_2^+, γ_3^+ (k_b^-, β_1^-, β_2^-, γ_1^-, γ_2^-, γ_3^-) can be arbitrary real numbers.

In addition, at the generic time t, the generalized tangent stiffness k_t can be evaluated as:

$$k_t(t) = k_e(t) + k_b + s(t)\alpha\left[f_e(t_P) + k_b u(t_P) + s(t)f_0 - f_{ri}(t_P)\right] e^{-s(t)\alpha(u(t)-u(t_P))}, \quad (16)$$

where:

$$k_e(t) = \beta_1\beta_2 e^{\beta_2 u(t)} + \frac{4\gamma_1\gamma_2 e^{-\gamma_2(u(t)-\gamma_3)}}{\left[1+e^{-\gamma_2(u(t)-\gamma_3)}\right]^2}. \quad (17)$$

In Equations (14) and (16), the generalized force $f_{ri}(t_P)$ is assumed to be assigned or evaluated at time $t_P < t$.

The expression providing the generalized work W_{ri} performed by f_{ri} over a generic generalized displacement interval is omitted for brevity and can be found in [8].

Table 1
VRM parameters adopted for the hysteresis loops in Figure 2.

Figure	s	k_b	f_0	α	β_1	β_2	γ_1	γ_2	γ_3
2a	$+$	0.5	2.0	10	0.0	0.0	0.0	0.0	0.0
	$-$	0.0	2.0	10	0.0	0.0	0.0	0.0	0.0
2b	$+$	0.5	2.0	10	0.0	0.0	0.5	4.0	0.5
	$-$	0.5	2.0	10	0.0	0.0	0.5	4.0	-0.5
2c	$+$	0.5	1.0	10	0.0	0.0	2.0	2.0	0.0
	$-$	0.5	1.0	10	0.0	0.0	2.0	2.0	0.0
2d	$+$	0.5	1.0	10	0.0	0.0	2.0	40	0.0
	$-$	0.5	1.0	10	0.0	0.0	2.0	40	0.0

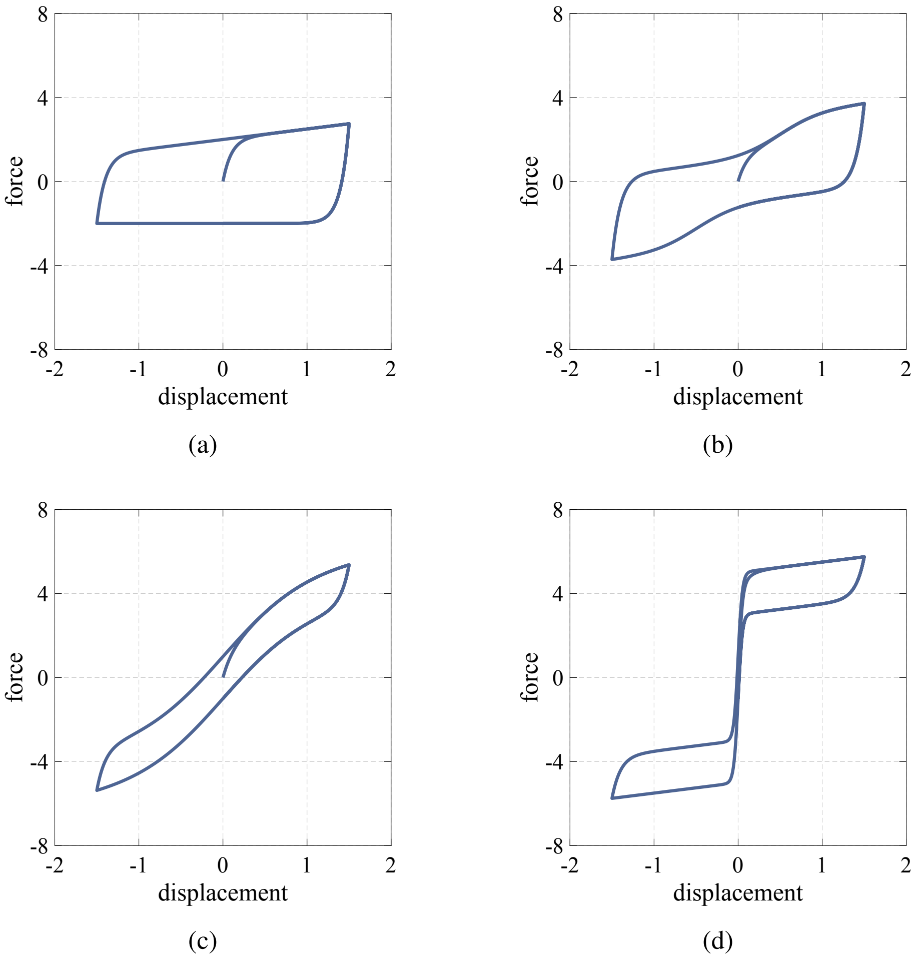

Figure 2: Examples of asymmetric (a), pinched (b), S-shaped (c), flag-shaped (d) hysteresis loops simulated by using the VRM parameters listed in Table 1.

3.2 Simulation of Complex Hysteresis Loops

Figure 2 illustrates four complex hysteresis loops simulated by adopting the model parameters listed in Table 1 and imposing a sinusoidal generalized displacement having an amplitude of 1.5 and a unit frequency.

Table 2
Coordinates of the vertices (in meters) defining the mathematical model in Figure 3a.

	P_1	P_2	P_3	P_4	P_5	P_6	P_7	P_8
x_1	0.4714	0.4714	-0.1286	-0.1286	-0.7286	-0.7286	-0.1286	-0.1286
x_2	-0.9429	1.0571	1.0571	0.2571	0.2571	-0.5429	-0.5429	-0.9429

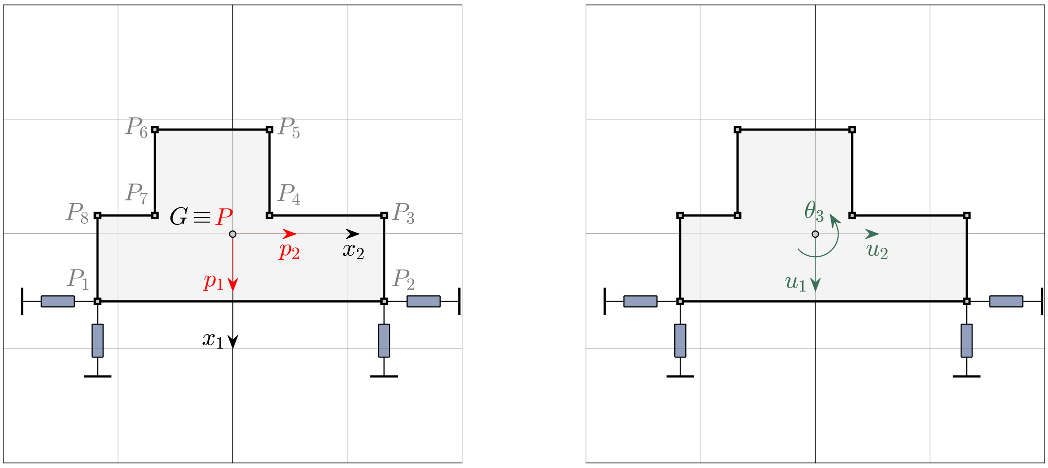

(a) (b)

Figure 3: Mathematical model (a) and selected generalized coordinates (b) adopted in the numerical experiment.

4 NUMERICAL EXPERIMENT

This section illustrates the results of a nonlinear dynamic analysis performed on a mechanical system equipped with four Wire Rope Isolators (WRIs) and subjected to bidirectional support acceleration. In particular, the type of devices adopted in the numerical simulation is denominated WRI PWHS16010 [12, 13].

To carry out the nonlinear time history analysis, the VRM, described in Section 3, is employed to simulate the behavior of each device along its axial and shear directions. Furthermore, an accurate and computationally efficient explicit time integration method, described in [14], is adopted to numerically integrate the system of nonlinear equilibrium equations provided by Equation (11). Due to its explicit nature, such a method offers the advantage of performing nonlinear dynamic analyses without using iterative procedures.

Both the hysteretic model and the numerical method are implemented in the computer program MATLAB R2022a.

4.1 Mathematical Model

Figure 3a shows the mathematical model of the mechanical system selected to perform the numerical experiment. In particular, it consists of a rigid body having polygonal shape and a uniformly distributed mass m; consequently, its mass center coincides with its gravity center G.

Table 2 presents the coordinates of the $N = 8$ vertices defining the domain Ω associated with the rigid body; they are numbered in consecutive order by circulating along the boundary in a counterclockwise sense and are defined with reference to a right-handed Cartesian coordinate

Table 3
VRM parameters adopted for the hysteresis loops in Figure 4.

Figure	s	k_b [N/m]	f_0 [N]	α [1/m]	β_1 [N]	β_2 [1/m]	γ_1 [N]	γ_2 [1/m]	γ_3 [m]
4a	$+$	500000	-500	1800	2500	230	0	0	0
	$-$	550000	4215	1700	1400	200	0	0	0
4b	$+$	220000	1150	680	100	300	0	0	0
	$-$	240000	1044	700	-100	-300	0	0	0

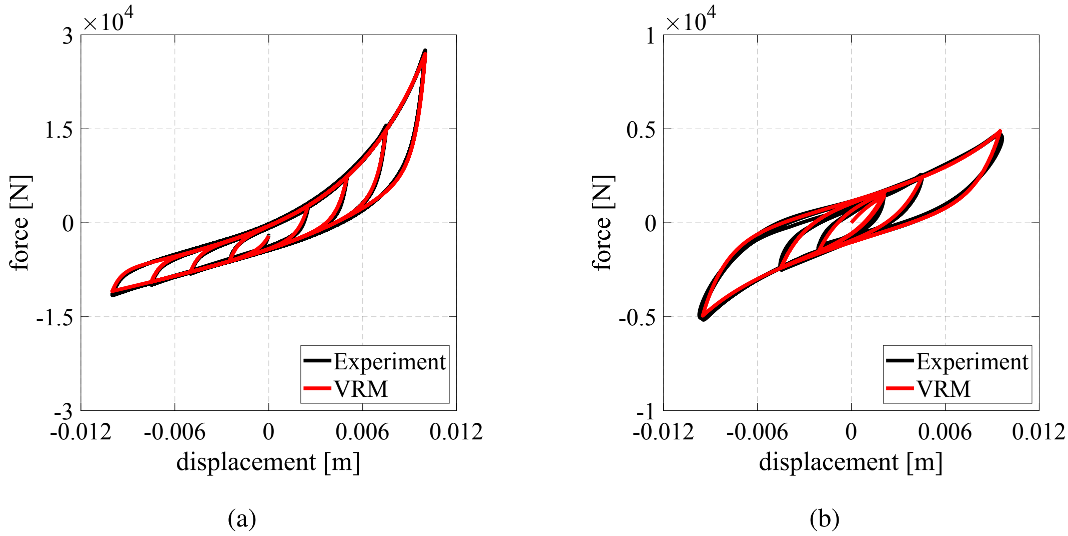

Figure 4: Comparison between experimental and analytical hysteresis loops exhibited by a single WRI along its axial (a) and shear (b) directions.

system having axes x_1, x_2, x_3 and origin at G.

The mass m of the rigid body is assumed to be equal to $815.7730\ \mathrm{Ns^2m^{-1}}$, whereas its second mass moment J_{x_3}, evaluated by using Equation (1), is equal to $297.7294\ \mathrm{Ns^2m}$.

Figure 3b illustrates the three generalized coordinates, namely u_1, u_2, θ_3, adopted to describe the rigid body motion.

To simulate the response exhibited by the two WRIs mounted under point P_1 (P_2), a set of four rate-independent hysteretic elements are attached to P_1 (P_2). Two of them are parallel to x_1 axis and simulate the devices axial response, whereas the other two are parallel to x_2 axis and simulate the devices shear response.

4.2 Hysteretic Model Parameters

The complex experimental behavior exhibited by each WRI, along the axial and shear directions, is simulated by using the VRM presented in Section 3.

Figure 4a (Figure 4b) compares the experimental hysteresis loops, describing the response of a single device along its axial (shear) direction for a frequency of 1 Hz and an axial load of 2 kN, with those predicted by means of the proposed hysteretic model. The adopted model parameters, identified on the basis of the experimental data, are listed in Table 3.

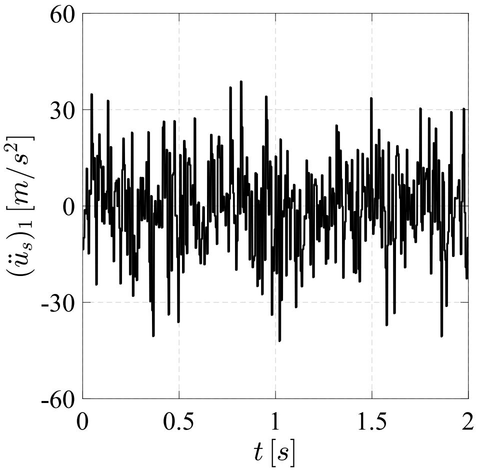

(a)

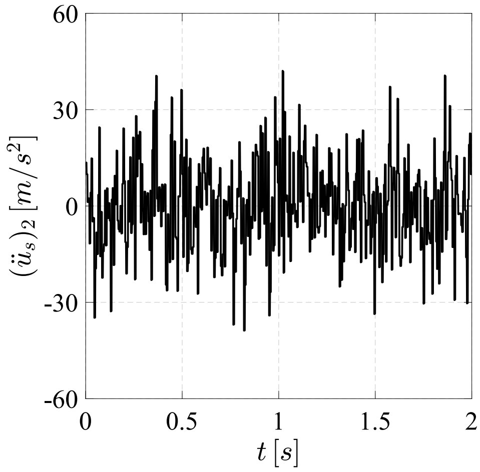

(b)

Figure 5: Time history of the support accelerations applied along x_1 (a) and x_2 (b) axes.

4.3 Applied Support Motion

The nonlinear time history analysis is performed by imposing, along the x_1 (x_2) axis, the support acceleration $(\ddot{u}_s)_1$ ($(\ddot{u}_s)_2$) illustrated in Figure 5a (Figure 5b) and by adopting a time step of 0.001 s. Specifically, the external force $p_1 = m(\ddot{u}_s)_1$ ($p_2 = m(\ddot{u}_s)_2$) is applied to point $G \equiv P$, as shown in Figure 3a.

4.4 Numerical Results

Figures 6a and 6b (Figures 7a and 7b) illustrate, respectively, the time history of the relative displacement u_1 (u_2) and total acceleration $(\ddot{u}_t)_1$ ($(\ddot{u}_t)_2$) of the mass center along x_1 (x_2) axis. In addition, Figures 8a and 8b show, respectively, the time history of the relative rotation θ_3 and total rotational acceleration $(\ddot{\theta}_t)_3$ of the rigid body about x_3 axis.

5 CONCLUSIONS

We have presented a mathematical model suitable for the nonlinear time history analysis of rigid bodies with arbitrary polygonal shape mounted on rate-independent hysteretic devices.

The force-displacement hysteresis loops, characterizing the response of such devices, have been simulated by using a recently formulated analytical hysteretic model, denominated Vaiana-Rosati model. Such a model has been selected, among others available in the literature, since it is able to reproduce complex hysteresis loop shapes, such as the asymmetric, pinched, S-shaped, flag-shaped ones or those obtained as their arbitrary combination.

A numerical experiment has been presented to illustrate the capability of the proposed mathematical model of simulating the dynamic response of a rigid body supported by four wire rope isolators and subjected to bidirectional support acceleration.

Acknowledgments

The present work was performed in the framework of ReLUIS-DPC 2022-2024 Project (WP 15, Tasks 15.1 and 15.2) and in the context of the research activities carried out by the GNFM (Gruppo Nazionale per la Fisica Matematica).

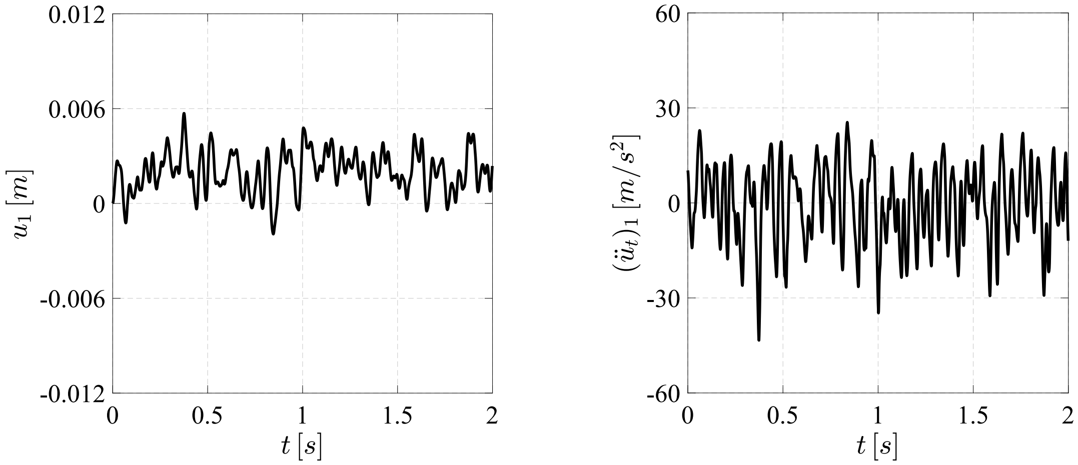

(a) (b)

Figure 6: Time history of the relative displacement u_1 (a) and total acceleration $(\ddot{u}_t)_1$ (b) of the mass center along x_1 axis.

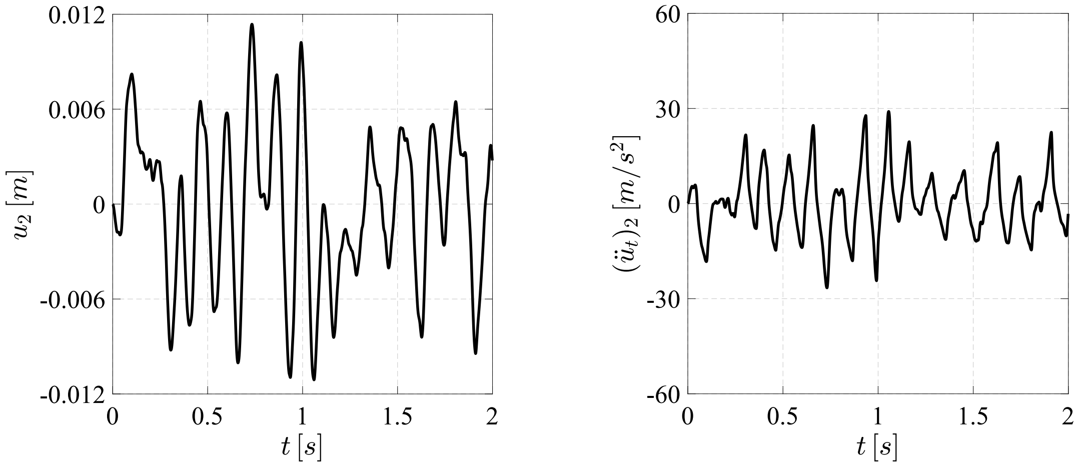

(a) (b)

Figure 7: Time history of the relative displacement u_2 (a) and total acceleration $(\ddot{u}_t)_2$ (b) of the mass center along x_2 axis.

References

[1] T.T. Soong, B.F. Spencer Jr, Supplemental energy dissipation: State-of-the-art and state-of-the-practice. *Engineering Structures*, **24**(3), 243–259, 2002.

[2] B. Carboni, W. Lacarbonara, Nonlinear vibration absorber with pinched hysteresis: Theory and experiments. *Journal of Engineering Mechanics*, **142**(5), 04016023, 2016.

[3] F. Cilento, D. Losanno, L. Piga, An experimental study on a novel reclaimed rubber compound for fiber-reinforced seismic isolators. *Structures*, **45**, 9–22, 2022.

[4] D. Losanno, D. De Domenico, I.E. Madera-Sierra, Experimental testing of full-scale fiber reinforced elastomeric isolators (FREIs) in unbounded configuration. *Engineering Structures*, **260**, 114234, 2022.

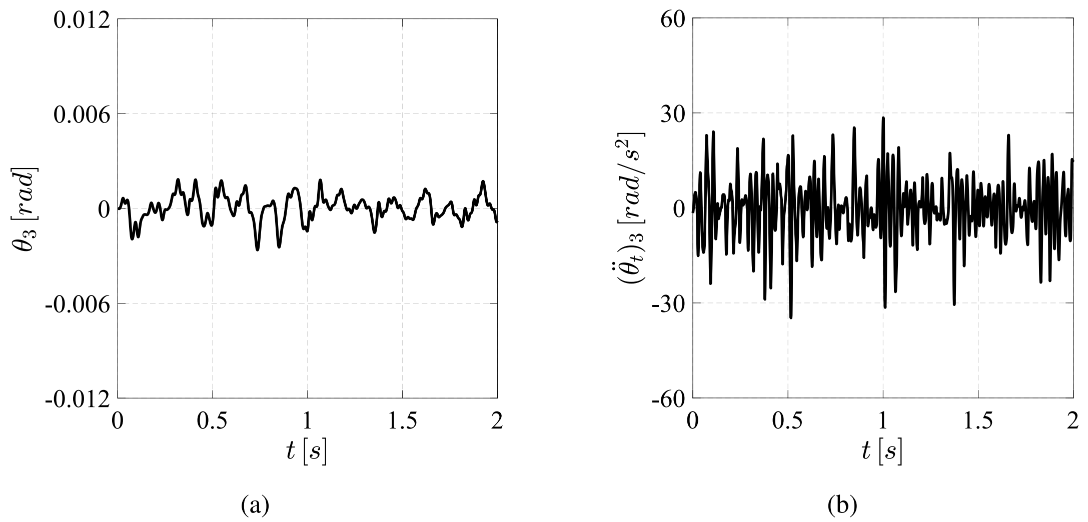

Figure 8: Time history of the relative rotation θ_3 (a) and total rotational acceleration $(\ddot{\theta}_t)_3$ (b) of the rigid body about x_3 axis.

[5] A. Orfeo, E. Tubaldi, A.H. Muhr, D. Losanno, Mechanical behaviour of rubber bearings with low shape factor. *Engineering Structures*, **266**, 114532, 2022.

[6] D. De Domenico, D. Losanno, N. Vaiana, Experimental tests and numerical modeling of full-scale unbonded fiber reinforced elastomeric isolators (UFREIs) under bidirectional excitation. *Engineering Structures*, **274**, 115118, 2023.

[7] N. Vaiana, L. Rosati, Classification and unified phenomenological modeling of complex uniaxial rate-independent hysteretic responses. *Mechanical Systems and Signal Processing*, **182**, 109539, 2023.

[8] N. Vaiana, R. Capuano, L. Rosati, Evaluation of path-dependent work and internal energy change for hysteretic mechanical systems. *Mechanical Systems and Signal Processing*, **186**, 109862, 2023.

[9] N. Vaiana, S. Sessa, F. Marmo, L. Rosati, A class of uniaxial phenomenological models for simulating hysteretic phenomena in rate-independent mechanical systems and materials. *Nonlinear Dynamics*, **93**(3), 1647–1669, 2018.

[10] N. Vaiana, S. Sessa, L. Rosati, A generalized class of uniaxial rate-independent models for simulating asymmetric mechanical hysteresis phenomena. *Mechanical Systems and Signal Processing*, **146**, 106984, 2021.

[11] N. Vaiana, D. Losanno, N. Ravichandran, A novel family of multiple springs models suitable for biaxial rate-independent hysteretic behavior. *Computers and Structures*, **244**, 106403, 2021.

[12] N. Vaiana, M. Spizzuoco, G. Serino, Wire rope isolators for seismically base-isolated lightweight structures: Experimental characterization and mathematical modeling. *Engineering Structures*, **140**, 498–514, 2017.

[13] D. Pellecchia, N. Vaiana, M. Spizzuoco, G. Serino, L. Rosati, Axial hysteretic behaviour of wire rope isolators: Experiments and modelling. *Materials and Design*, **225**, 111436, 2023.

[14] N. Vaiana, S. Sessa, F. Marmo, L. Rosati, Nonlinear dynamic analysis of hysteretic mechanical systems by combining a novel rate-independent model and an explicit time integration method. *Nonlinear Dynamics*, **98**(4), 2879–2901, 2019.